Research report on unified stochastic reverberation modeling

Modèle stochastique unifié de réverbération

Roland Badeau

2018D001

février 2018

Département Image, Données, Signal
Groupe S^2A : Signal, Statistiques et Apprentissage

Research report on unified stochastic reverberation modeling
Modèle stochastique unifié de réverbération

Roland Badeau
LTCI, Télécom ParisTech, Université Paris-Saclay, Paris, France
Email: roland.badeau@telecom-paristech.fr

***Abstract*—In the field of room acoustics, it is well known that reverberation can be characterized statistically in a particular region of the time-frequency domain (after the mixing time and above Schroeder's frequency). Since the 1950s, various formulas have been established, focusing on particular aspects of reverberation: exponential decay over time, correlations between frequencies, correlations between sensors at each frequency, and time-frequency distribution. In this report, we introduce a new stochastic reverberation model, that permits us to retrieve all these well-known results within a common mathematical framework. To the best of our knowledge, this is the first time that such a unification work is presented. The benefits are multiple: several new formulas generalizing the classical results are established, that jointly characterize the spatial, temporal and spectral properties of late reverberation.**

***Index Terms*—Reverberation, room impulse response, room frequency response, stochastic models, Poisson processes, stationary processes, Wigner distribution.**

***Résumé*—Dans le domaine de l'acoustique des salles, il est connu que la réverbération peut être caractérisée statistiquement dans une région particulière du domaine temps-fréquence (après le temps de mélange et au-dessus de la fréquence de Schroeder). Depuis les années 50, diverses formules ont été établies, portant sur des aspects particuliers de la réverbération : la décroissance exponentielle au cours du temps, les corrélations entre fréquences, les corrélations entre capteurs à chaque fréquence, et la distribution temps-fréquence.**

Dans ce rapport, nous introduisons un nouveau modèle stochastique de réverbération, qui nous permet de retrouver tous ces résultats déjà connus dans un cadre mathématique commun. À notre connaissance, c'est la première fois qu'un tel travail d'unification est présenté. Les bénéfices en sont multiples : plusieurs formules nouvelles généralisant les résultats classiques sont établies, qui caractérisent conjointement les propriétés spatiales, temporelles et spectrales de la réverbération tardive.

***Mots clés*—Réverbération, réponse impulsionnelle de salle, réponse fréquentielle de salle, modèles stochastiques, processus de Poisson, processus stationnnaires, distribution de Wigner-Ville.**

I. Introduction

When a microphone records a sound produced by an audio source in a room, the received signal is made of several contributions [1]: firstly, the *direct sound*, that corresponds to the direct propagation of the sound wave from the source to the microphone, then a few *early reflections*, that are due to the sound wave reflections on the various room surfaces (walls, floor, ceiling…), and finally the *late reverberation*: after a time called *mixing time* [2], [3], reflections are so frequent that they form a continuum and, because the sound is partially *absorbed* by the room surfaces at every reflection, the sound level decays exponentially over time. This phenomenon is called *reverberation*, and it can be modeled as the convolution between the source signal and a causal *room impulse response* (RIR), made of a few isolated impulses before the mixing time, and of a continuous, exponentially decaying, random process in late reverberation. The Fourier transform of the RIR is called *room frequency response* (RFR), and the modal theory [4] shows that its profile is qualitatively similar to that of the RIR: below a frequency called *Schroeder's frequency*, the RFR is made of a few isolated modes, and above this frequency the modes become so dense that they can be represented as a continuous random process [5]–[7].

To sum up, reverberation can be modeled as a stochastic process in a rectangular region of the time-frequency domain [8], as depicted[1] in Fig. 1.

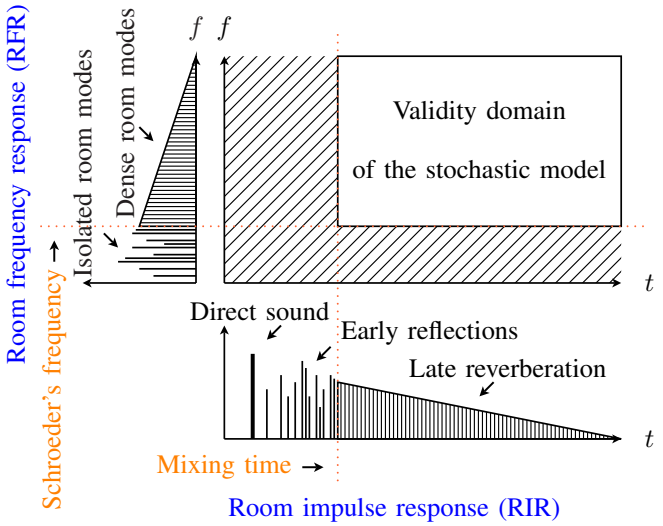

Fig. 1. Time-frequency profile of reverberation

If in addition the dimensions of the room are much larger than the wavelength, and the source and the microphones are

[1]Fig. 1 is adapted from [8, p. 30] and [9, p. 20].

located at least a half-wavelength away from the walls, then in this time-frequency region, the sound field can generally be approximated as *diffuse* [10]–[12]. Diffusion is a consequence of the reflections on the room surfaces not being *specular* (*i.e.* mirror-like), but rather *scattered* in various directions, as represented in Fig. 2. After many reflections, the sound field can be considered as *isotropic*: the sound waves come uniformly from all directions.

Historically, the first stochastic reverberation model is due to Schroeder [5] and Moorer [13]: the RIR at microphone i is

$$h_i(t) = b_i(t)e^{-\alpha t}\mathbf{1}_{t\geq 0} \tag{1}$$

where $\alpha > 0$ and $b_i(t)$ is a centered white Gaussian process. Parameter α is related to the reverberation time T_r in seconds by the equation $T_r = \frac{3\ln(10)}{\alpha}$. The Gaussian distribution of $b_i(t)$ arises from the central limit theorem: in late reverberation, $h_i(t)$ is the sum of many independent contributions.

Schroeder [5]–[7] also noticed that the independency of the samples $h_i(t)$ implies that the RFR, defined as their Fourier transform[2] $\mathcal{F}_{h_i}(f)$, is a stationary random process. From (1), he derived several formulas that can be summarized by expressing the complex autocorrelation function[3] of $\mathcal{F}_{h_i}(f)$:

$$\operatorname{corr}\left[\mathcal{F}_{h_i}(f_1),\, \mathcal{F}_{h_i}(f_2)\right] = \frac{1}{1+\imath\pi\frac{f_1-f_2}{\alpha}}. \tag{2}$$

Following a similar approach in the spectral domain, under the diffuse field assumption, Cook [14] computed the correlation at frequency f between two sensors at distance D:

$$\operatorname{corr}\left[\mathcal{F}_{h_1}(f),\, \mathcal{F}_{h_2}(f)\right] = \operatorname{sinc}\left(\frac{2\pi f D}{c}\right). \tag{3}$$

Equation (3) was later generalized to combinations of pressure and velocity sensors [15] and to differential microphones [16].

Finally, Polack [17] generalized model (1) by assuming that $b_i(t)$ is a centered stationary Gaussian process, whose power spectral density (PSD) $B(f)$ has slow variations[4]. Then he showed that the Wigner distribution[5] [18] of the RIR is

$$\mathcal{W}_{h_i,h_i}(t,f) = B(f)e^{-2\alpha t}\mathbf{1}_{t\geq 0}. \tag{4}$$

In order to account for the fact that the attenuation coefficient α actually depends on the frequency f, he also proposed an empirical generalization of (4):

$$\mathcal{W}_{h_i,h_i}(t,f) = B(f)e^{-2\alpha(f)t}\mathbf{1}_{t\geq 0}. \tag{5}$$

In other respects, based on the billiard theory, Polack [2], [3] also showed that the durations of the various trajectories in a room, from a given source position to the microphone, are distributed according to a Poisson process [19].

In this report, we propose a unified stochastic model of reverberation, that will permit us to retrieve all formulas (1) to (4) in a common mathematical framework[6], to establish a link with the Poisson distribution proposed by Polack, and to show how the probability distribution of the RIR, which is impulsive in early reverberation, converges to the Gaussian distribution in late reverberation. In addition, this model will also permit us to go deeper into the description of the statistical properties of the RIR over the space, time and frequency domains, and to prove several new results.

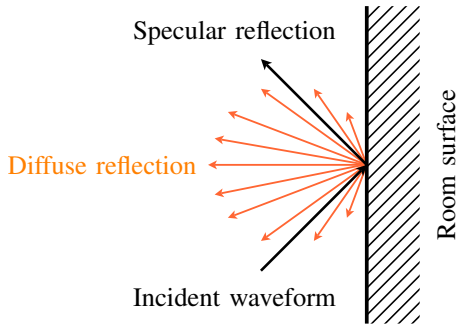

Fig. 2. Specular vs. diffuse reflection

This report is structured as follows: Section II presents important mathematical definitions and notation that will be used throughout the report. Then our general stochastic reverberation model is introduced in Section III. The statistical properties of this model at one sensor are investigated in Section IV. The statistical relationships between two sensors are then analyzed in Section V. Finally, some conclusions and perspectives are presented in Section VI. Note that this is a fully theoretical work: our purpose was to unify several results that have already been validated experimentally. In order to make the main discussion as clear as possible, all mathematical proofs were moved to Appendices A to C.

II. Mathematical definitions

- $\mathbb{N}$: set of whole numbers
- $\mathbb{R}$, $\mathbb{C}$: sets of real and complex numbers, respectively
- $\mathbb{R}_+$: set of nonnegative real numbers
- $\imath = \sqrt{-1}$: imaginary unit
- $[a,b]$: closed interval, including a and $b \in \mathbb{R}$
- $]a,b[$: open interval, excluding a and $b \in \mathbb{R}$
- $L^2([a,b])$: square-integrable functions of support $[a,b]$
- δ: Dirac delta function
- $\boldsymbol{x}$ (bold font), z (regular): vector and scalar, respectively
- $\|.\|_2$: Euclidean/Hermitian norm of a vector or a function
- $\overline{z}$: complex conjugate of $z \in \mathbb{C}$
- $\boldsymbol{x}^\top$: transpose of vector $\boldsymbol{x}$
- $\mathcal{S}^2$: unit sphere in $\mathbb{R}^3$ ($\mathcal{S}^2 = \{\boldsymbol{x} \in \mathbb{R}^3; \|\boldsymbol{x}\|_2 = 1\}$)
- $\mathbb{E}[X]$: expected value of a random variable X
- $\phi_X(\theta) = \mathbb{E}[e^{\imath\theta X}]$: characteristic function of X
- Covariance of two complex random variables X and Y:

$$\operatorname{cov}[X,Y] = \mathbb{E}[(X-\mathbb{E}[X])\overline{(Y-\mathbb{E}[Y])}] \tag{6}$$

[2]The Fourier transform is defined in equation (9).
[3]The correlation of two complex random variables is defined in equation (7).
[4]Note that in this case, $\mathcal{F}_{h_i}(f)$ is no longer a stationary process.
[5]The Wigner distribution is defined in equation (11).
[6]A straightforward generalization of this model also permits to prove (5), that will be presented in a future paper; a few hints will be given in Section VI.

- $\mathrm{var}[X] = \mathrm{cov}[X, X]$: variance of a random variable X
- Correlation of two complex random variables X and Y:

$$\mathrm{corr}[X, Y] = \frac{\mathrm{cov}[X, Y]}{\sqrt{\mathrm{var}[X]\,\mathrm{var}[Y]}} \tag{7}$$

- $\mathcal{P}(\lambda)$: Poisson distribution of parameter $\lambda > 0$:

$$N \sim \mathcal{P}(\lambda) \Leftrightarrow P(N{=}n) = e^{-\lambda}\frac{\lambda^n}{n!} \Leftrightarrow \phi_N(\theta) = e^{\lambda(e^{\imath\theta}-1)} \tag{8}$$

- $\mathrm{sinc}(x) = \frac{\sin(x)}{x}$: cardinal sine function
- $\mathbf{1}_A$: indicator function ($\mathbf{1}_A(x)$ is 1 if $x \in A$ or 0 if $x \notin A$)
- $\widetilde{\psi}(t) = \overline{\psi(-t)}$: conjugate and time-reverse of $\psi : \mathbb{R} \to \mathbb{C}$
- Convolution of two functions ψ_1 and $\psi_2 : \mathbb{R} \to \mathbb{C}$:

$$(\psi_1 * \psi_2)(t) = \int_{u\in\mathbb{R}} \psi_1(u)\psi_2(t-u)du$$

- Fourier transform of a function $\psi : \mathbb{R} \to \mathbb{C}$:

$$\mathcal{F}_\psi(f) = \int_{t\in\mathbb{R}} \psi(t)e^{-2\imath\pi ft}dt \quad (f \in \mathbb{R}) \tag{9}$$

- Two-sided Laplace transform of a function $\psi : \mathbb{R} \to \mathbb{C}$:

$$\mathcal{L}_\psi(s) = \int_{t\in\mathbb{R}} \psi(t)e^{-st}dt \quad (s \in \mathbb{C}) \tag{10}$$

- Wigner distribution (*a.k.a.* Wigner-Ville distribution) of two second-order random processes $\psi_1(t)$ and $\psi_2(t)$:

$$\mathcal{W}_{\psi_1,\psi_2}(t, f) = \int_{\mathbb{R}} \mathrm{cov}[\psi_1(t+\tfrac{u}{2}),\, \psi_2(t-\tfrac{u}{2})]e^{-2\imath\pi fu}du. \tag{11}$$

III. Definition of the stochastic model

The model that we present in this section is based on the source image principle [1], [20]. As illustrated in Fig. 3 in the case of specular reflections in a rectangular room[7], the trajectory inside the room from the real source to the microphone is equivalent to a virtual straight trajectory from a so-called *source image* which is outside the room. A remarkable property of this principle is that, regardless of the room dimensions, the density of the source images is uniform in the whole space: the number of source images contained in a given disk, of radius sufficiently larger than the room dimensions, is approximately invariant under any translation of this disk.

Since we aim to define a general stochastic reverberation model, independent of the geometry of the room, we will consider that the positions of the source images are random and uniformly distributed (note that this assumption is *a fortiori* valid in the case of a diffuse sound field, which is uniform). More precisely, we will assume that the number $N(V)$ of source images contained in any Borel set $V \subset \mathbb{R}^3$ follows a Poisson distribution[8] of parameter $\lambda|V|$, where $|V|$ is the Lebesgue measure (volume) of V. Mathematically, this is formalized by considering a Poisson random measure with independent increments $dN(\boldsymbol{x}) \sim \mathcal{P}(\lambda d\boldsymbol{x})$.

[7]Fig. 3 illustrates the source image principle in 2D-space for convenience, but of course our model will be defined in the 3D-space.

[8]The Poisson distribution is defined in equation (8).

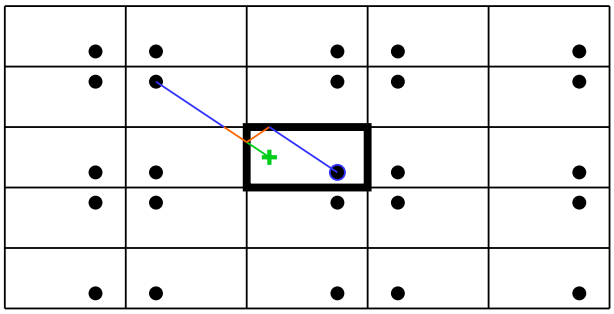

Fig. 3. Positions of microphone (green plus), source (thick blue point) and source images (black points). The original room walls are drawn with thick lines. A virtual straight trajectory from one source image to the microphone is drawn with colors, along with the real trajectory in the original room.

In other respects, we will assume that the sound waves undergo an exponential attenuation along their trajectories, that is due to the multiple reflections on the room surfaces and to the propagation in the air. In this report we focus on the case of omnidirectional microphones, so we will further assume that this attenuation is isotropic (in accordance with the diffuse field approximation) and independent of the frequency. It will thus only depend on the length of the trajectory, as in [17].

Finally, we suppose that several microphones[9] indexed by an integer i are placed at arbitrary positions $\boldsymbol{x}_i$ in the room.

We end up with the following model:

$$h_i(t) = \int_{\boldsymbol{x}\in\mathbb{R}^3} h_i(t, \boldsymbol{x})\, e^{-\frac{\alpha}{c}\|\boldsymbol{x}-\boldsymbol{x}_i\|_2}\, dN(\boldsymbol{x}), \tag{12}$$

where $h_i(t)$ is the RIR at microphone i, $\alpha > 0$ is the attenuation coefficient (in Hz), and $c > 0$ is the sound speed in the air (approximately 340 m/s in usual conditions). The impulse $h_i(t, \boldsymbol{x})$, propagated from the source image at position $\boldsymbol{x}$, is modeled as a coherent sum of monochromatic spherical waves:

$$h_i(t, \boldsymbol{x}) = \int_{f\in\mathbb{R}} A_i(f)\frac{e^{2\imath\pi f\left(t-\frac{\|\boldsymbol{x}-\boldsymbol{x}_i\|_2}{c}\right)}}{\|\boldsymbol{x}-\boldsymbol{x}_i\|_2}df, \tag{13}$$

where $A_i(f)$ is a linear-phase frequency response (in order to ensure coherence). In Appendix A , we show that (12) and (13) are equivalent to the following model:

Definition 1 (Unified stochastic reverberation model)**.** *Let $\alpha > 0$, $c > 0$, and $T > 0$. Let $dN(\boldsymbol{x})$ be a uniform Poisson random measure on $\mathbb{R}^3$ with independent increments:*

$$dN(\boldsymbol{x}) \sim \mathcal{P}(\lambda d\boldsymbol{x}). \tag{14}$$

Let $g(t) \in L^2([-T, T])$, such that

$$\mathcal{F}_g(0) = \frac{d\mathcal{F}_g}{df}(0) = 0, \tag{15}$$

$$\forall f \in \mathbb{R},\ \mathcal{L}_g(\alpha + 2\imath\pi f) \geq 0. \tag{16}$$

At any sensor position $\boldsymbol{x}_i \in \mathbb{R}^3$, $h_i(t)$ is defined as

$$\forall t \in \mathbb{R},\ h_i(t) = e^{-\alpha(t-T)}\, b_i(t), \tag{17}$$

[9]For the sake of simplicity, we will focus on the case of two microphones; the generalization to an arbitrary number of microphones is straightforward.

where

$$b_i(t) = \int_{\boldsymbol{x}\in\mathbb{R}^3} g\left(t - T - \frac{\|\boldsymbol{x}-\boldsymbol{x}_i\|_2}{c}\right)\frac{dN(\boldsymbol{x})}{\|\boldsymbol{x}-\boldsymbol{x}_i\|_2}. \quad (18)$$

Equivalently, the Fourier transform of $h_i(t)$ is

$$\mathcal{F}_{h_i}(f) = \mathcal{L}_g(\alpha+2\imath\pi f)e^{-2\imath\pi fT}\int_{\mathbb{R}^3}\frac{e^{-\frac{\alpha+2\imath\pi f}{c}\|\boldsymbol{x}-\boldsymbol{x}_i\|_2}}{\|\boldsymbol{x}-\boldsymbol{x}_i\|_2}dN(\boldsymbol{x}). \quad (19)$$

This definition calls for comments. Firstly, the linear-phase frequency response $A_i(f)$ in (13) was parameterized as

$$A_i(f) = \mathcal{L}_g(\alpha+2\imath\pi f)e^{-2\imath\pi fT}. \quad (20)$$

This technical definition aims to simplify the mathematical developments in the next sections. Secondly, any function $g \in L^2([-T,T])$ is such that $\mathcal{F}_g(f)$ and $f \mapsto \mathcal{L}_g(\alpha+2\imath\pi f)$ are infinitely differentiable, so $\mathcal{F}_g(0)$, $\frac{d\mathcal{F}_g}{df}(0)$ and $\mathcal{L}_g(\alpha+2\imath\pi f)$ are well-defined. The constraints (15) and (16) imposed to g are required to prove Propositions 2 and 3 in Sections IV and V. In particular, the support of g is chosen so that $h_i(t)$ in (17) and $b_i(t)$ in (18) are causal. Thirdly, the existence of functions g that satisfy these constraints is guaranteed by Lemma 1 in Appendix A.

Now it is time to investigate the properties of this model. In Section IV, we will focus on one sensor at spatial position $\boldsymbol{x}_i$. Then in Section V, we will analyze the spatial relationships between two sensors at different positions $\boldsymbol{x}_i$ and $\boldsymbol{x}_j$.

IV. Statistical properties at one sensor

Let us first introduce an equivalent model definition:

Proposition 1 (Equivalent model definition at one sensor)**.** *With the same notation as in Definition 1, we have:*

$$b_i(t) = \int_{r\in\mathbb{R}_+} g\left(t - T - \frac{r}{c}\right)\frac{dN(r)}{r}, \quad (21)$$

$$\mathcal{F}_{h_i}(f) = \mathcal{L}_g(\alpha+2\imath\pi f)e^{-2\imath\pi fT}\int_{r\in\mathbb{R}_+}\frac{e^{-\frac{\alpha+2\imath\pi f}{c}r}dN(r)}{r} \quad (22)$$

where $dN(r)$ are independent Poisson increments on $\mathbb{R}_+$:

$$dN(r) \sim \mathcal{P}(4\pi\lambda r^2 dr). \quad (23)$$

Proposition 1 is proved in Appendix A. Let us now investigate the statistical properties of this model:

Proposition 2 (Statistical properties at one sensor position)**.** *The model in Definition 1 has the following properties:*

1) *First order moments:*
   - *in the spectral domain: $\forall f \in \mathbb{R}$,*

$$\mathbb{E}[\mathcal{F}_{h_i}(f)] = \frac{4\pi\lambda c^2\mathcal{L}_g(\alpha+2\imath\pi f)\,e^{-2\imath\pi fT}}{(\alpha+2\imath\pi f)^2}, \quad (24)$$

   - *in the time domain:*

$$\forall t \geq 2T,\ \mathbb{E}[h_i(t)] = \mathbb{E}[b_i(t)] = 0. \quad (25)$$

2) *Second order moments:*
   - *in the spectral domain: $\forall f, f_1, f_2 \in \mathbb{R}$,*

$$\mathrm{var}[\mathcal{F}_{h_i}(f)] = 2\pi\lambda c\,\mathcal{L}_g(\alpha+2\imath\pi f)^2/\alpha, \quad (26)$$

$$\mathrm{corr}[\mathcal{F}_{h_i}(f_1),\mathcal{F}_{h_i}(f_2)] = \frac{e^{-2\imath\pi(f_1-f_2)T}}{1+\imath\pi\frac{f_1-f_2}{\alpha}}. \quad (27)$$

   - *in time domain: $\forall t \geq 2T$, $b_i(t)$ is a wide sense stationary (WSS) process, of autocovariance function*

$$\forall\tau\in\mathbb{R}, \Gamma(\tau) = \mathrm{cov}[b_i(t+\tau),b_i(t)] = 4\pi\lambda c\,\widetilde{g}*g(\tau) \quad (28)$$

   autocorrelation function

$$\forall\tau\in\mathbb{R},\ \gamma(\tau) = \mathrm{corr}[b_i(t+\tau),b_i(t)] = \frac{(\widetilde{g}*g)(\tau)}{\|g\|_2^2} \quad (29)$$

   and power spectral density

$$\forall f\in\mathbb{R},\ B(f) = \mathcal{F}_\Gamma(f) = 4\pi\lambda c\,|\mathcal{F}_g(f)|^2. \quad (30)$$

   Consequently,

$$\forall t \geq 2T,\ \mathrm{var}[h_i(t)] = 4\pi\lambda c\|g\|_2^2\,e^{-2\alpha(t-T)} \quad (31)$$

$$\forall t_1,t_2 \geq 2T, \mathrm{corr}[h_i(t_1),h_i(t_2)] = \gamma(t_1-t_2) \quad (32)$$

   - *in the time-frequency domain:*

$$\forall f\in\mathbb{R}, \forall t\geq 2T,\ \mathcal{W}_{h_i,h_i}(t,f) = B(f)\,e^{-2\alpha(t-T)}. \quad (33)$$

3) *Asymptotic normality: when $t \to +\infty$ (i.e. $t \gg T$), $b_i(t)$ is distributed as a stationary Gaussian process.*

Proposition 2 is proved in Appendix B. Note that (30) and (15) show that $B(f)$ is very flat at $f = 0$: $B(0) = \frac{dB}{df}(0) = \frac{d^2B}{df^2}(0) = \frac{d^3B}{df^3}(0) = 0$. The asymptotic normality is related to the central limit theorem: when r becomes large, the volume contained between the spheres of radius r and $r+dr$ increases as r^2dr, and so does the number of source images included in this volume as shown in (23), which leads to the addition of an increasing number of independent and identically distributed (i.i.d.) random increments $dB(x)$.

This proposition permits us to retrieve most of the classical results listed in the introduction. Firstly, $h_i(t)$ is centered for $t \geq 2T$ (the fact that it is *not* centered for $t \in [0,2T]$ explains why the expected value of the frequency response $\mathbb{E}[\mathcal{F}_{h_i}(f)]$ in (24) is not zero). Secondly, (17) corresponds to Schroder and Moorer's model defined in (1) when $T \to 0$ (in this case the process $b_i(t)$ becomes white, and it is Gaussian when $t \gg T$), and in the general case it is equivalent to Polack's model [17, chap. 1] ($b_i(t)$ is a centered stationary Gaussian process when $t \gg T$). When $T \to 0$, (27) reduces to Schroeder's formula (2), which was indeed established by assuming that $b_i(t)$ is white. Finally, (33) is equivalent to Polack's time-frequency model defined in (4). To the best of our knowledge, the other formulas in Proposition 2 are novel.

V. Statistical properties between two sensors

Let us now focus on the relationships between two sensors:

Proposition 3 (Statistical properties between two sensors)**.** *Let us consider the model in Definition 1 at two positions $\boldsymbol{x}_i$ and $\boldsymbol{x}_j \in \mathbb{R}^3$. Let us define the rectangular window*

$$\forall t \in \mathbb{R},\ w(t) = \frac{c}{2D}\mathbf{1}_{[-\frac{D}{c},\frac{D}{c}]}(t), \tag{34}$$

where $D = \|\boldsymbol{x}_i - \boldsymbol{x}_j\|_2$. Then, in addition to the properties listed in Proposition 2, we also have:

- *in the spectral domain: $\forall f_1, f_2 \in \mathbb{R}$,*

$$\operatorname{corr}[\mathcal{F}_{h_i}(f_1), \mathcal{F}_{h_j}(f_2)] = \frac{e^{-\frac{\alpha D}{c} - 2\imath\pi(f_1-f_2)(T+\frac{D}{2c})}\operatorname{sinc}(\frac{\pi(f_1+f_2)D}{c})}{1+\imath\pi\frac{f_1-f_2}{\alpha}} \tag{35}$$

- *in the time domain: $\forall t \geq 2T+\frac{D}{c}$, $\boldsymbol{b}(t) = [b_i(t), b_j(t)]^\top$ is a centered WSS process, of cross-autocovariance function*

$$\forall \tau \in \mathbb{R}, \Gamma_{i,j}(\tau) = \operatorname{cov}[b_i(t+\tau), b_j(t)] = w * \Gamma(\tau) \tag{36}$$

cross-autocorrelation function

$$\forall \tau \in \mathbb{R}, \gamma_{i,j}(\tau) = \operatorname{corr}[b_i(t+\tau), b_j(t)] = w * \gamma(\tau) \tag{37}$$

and cross-power spectral density

$$\forall f \in \mathbb{R}, B_{i,j}(f) = \mathcal{F}_{\Gamma_{i,j}}(f) = B(f)\operatorname{sinc}(\frac{2\pi f D}{c}). \tag{38}$$

Consequently,

$$\forall t_1, t_2 \geq 2T+\tfrac{D}{c},\ \operatorname{corr}[h_i(t_1), h_j(t_2)] = w * \gamma\,(t_1 - t_2)\,. \tag{39}$$

- *in the time-frequency domain: $\forall f \in \mathbb{R}$,*

$$\forall t \geq 2T+\tfrac{D}{2c}, \mathcal{W}_{h_i,h_j}(t,f) = B(f)e^{-2\alpha(t-T)}\operatorname{sinc}(\tfrac{2\pi f D}{c}). \tag{40}$$

- *asymptotic normality: when $t \to +\infty$ (i.e. $t \gg T$), $\boldsymbol{b}(t)$ is distributed as a stationary Gaussian process.*

Proposition 3 is proved in Appendix C. Applying equation (35) to $f_1 = f_2 = f$, we get Cook's formula (3) when $\alpha \to 0$ (no exponential decay). This formula was indeed originally proved by considering plane waves under a far-field assumption [14]. Besides, equation (39) shows that $h_i(t)$ and $h_j(t)$ are correlated on a time interval that corresponds to the wave propagation from one sensor to the other. To the best of our knowledge, all formulas in Proposition 3 are novel.

VI. Conclusion and perspectives

In this report, we proposed a new stochastic model of reverberation, that permitted us to retrieve various well-known results within a common framework. This unification work resulted in several new results, that jointly characterize the properties of late reverberation in the space, time, and frequency domains. The most noticeable result in our opinion is (40), which very simply makes the connection between Polack's time-frequency model (4) and Cook's formula (3).

Although this model was motivated by physical assumptions that only hold in a particular region of the time-frequency domain (after the mixing time and above Schroeder's frequency), from a signal processing perspective however, one of its most interesting features is that it is also applicable *before* the mixing time and *below* Schroeder's frequency. Indeed, since the parameter of the Poisson distribution $dN(r)$ in (23) increases quadratically with the distance r, the model permits to describe both the impulsiveness of the RIR before the mixing time, and its asymptotic normality in late reverberation. Moreover, the frequency response $\mathcal{L}_g(\alpha+2\imath\pi f)$ in (19) is able to fit both the smooth PSD $B(f)$ at high frequencies, and sharp resonances due to isolated modes below Schroeder's frequency. Therefore we end up with a stochastic model involving very few parameters (α, λ, filter g, and the distances between microphones), that is able to accurately describe reverberation in the whole time-frequency domain. We thus believe that this model has an interesting potential in a variety of signal processing applications.

However this reverberation model, as it is presented in this report, is not yet suitable for modeling real RIRs. Indeed, one assumption has to be relaxed: the attenuation coefficient α is not constant but rather depends on frequency in practice, as in Polack's generalized time-frequency model (5). In a future paper, we will thus present a generalization of the proposed model where we will introduce a frequency-varying attenuation coefficient. Fortunately, a simplification holds asymptotically (in late reverberation), that makes all mathematical derivations still analytically tractable. In particular, we will be able to present a formula that generalizes both (5) and (40). A second generalization of this model would be to represent acoustic fields that are not perfectly diffuse. Apparently, obtaining a mathematical characterization of such acoustic fields should be feasible, because a similar simplification holds asymptotically. Finally, the generalization to directional microphones is straightforward, by using the same approach as presented in [16].

Our future contributions will also focus on the signal processing aspects of this work: we will show how the generalized model (with a frequency-varying attenuation coefficient) can be formalized in discrete time, and we will propose a fast algorithm that permits to estimate the model parameters with a complexity of $O(L\,\log(L)^2)$, where L is the length of the RIR in samples. Finally, our ultimate goal is to investigate the potential of this model in applications such as source separation, dereverberation, and synthetic reverberation.

Appendix A
Proofs for the definition of the stochastic model

The following lemma aims to prove the existence of functions g that satisfy conditions (15) and (16) in Definition 1.

Lemma 1. *Let $\psi(t) \in L^2([0,T])$ with $T > 0$, such that $\int_{t=0}^{T}\psi(t)e^{\alpha t}dt = \int_{t=0}^{T}\psi(t)e^{-\alpha t}dt = 0$, where $\alpha \in \mathbb{R}$. Let $g(t) = (\widetilde{\psi} * \psi)(t)\,e^{\alpha(t-T)}$. Then function g satisfies conditions* (15) *and* (16) *in Definition 1.*

Proof of Lemma 1. Since $\psi(t) \in L^2([0,T])$, function g is continuous and bounded. Firstly, $\mathcal{F}_g(f) = e^{-\alpha T}\overline{\mathcal{L}_\psi(\alpha+2\imath\pi f)}\mathcal{L}_\psi(-\alpha+2\imath\pi f)$. Moreover, since $\psi(t)$ has finite support, both functions $f \mapsto \mathcal{L}_\psi(-\alpha+2\imath\pi f)$ and $f \mapsto \mathcal{L}_\psi(\alpha+2\imath\pi f)$ are infinitely differentiable. In addition,

$\mathcal{L}_\psi(-\alpha) = \mathcal{L}_\psi(\alpha) = 0$, which finally proves (15). Secondly, $\mathcal{L}_g(\alpha + 2\imath\pi f) = e^{-\alpha T}|\mathcal{F}_\psi(f)|^2$, which proves (16). □

We can now derive equations (17), (18) and (19) in Definition 1. By substituting (13) and (20) into (12), we get

$$\begin{aligned} h_i(t) = \quad & \int_{f\in\mathbb{R}} \mathcal{L}_g(\alpha + 2\imath\pi f) e^{2\imath\pi f(t-T)} \\ & \int_{\boldsymbol{x}\in\mathbb{R}^3} \frac{e^{-\frac{\alpha+2\imath\pi f}{c}\|\boldsymbol{x}-\boldsymbol{x}_i\|_2}}{\|\boldsymbol{x}-\boldsymbol{x}_i\|_2} dN(\boldsymbol{x})\, df \end{aligned}$$

which shows that $h_i(t)$ as defined in (12) is the inverse Fourier transform of (19) and therefore proves (19). Besides, applying the Fourier transform (9) to (17) also leads to (19), which proves the equivalence between (17)-(18), and (12)-(13)-(20).

Finally, let us prove Proposition 1.

Proof of Proposition 1. Let $dN(r) = \int_{\boldsymbol{u}\in\mathcal{S}^2} dN(r\boldsymbol{u})$. Then (14) implies (23). The change of variables $\boldsymbol{x} = \boldsymbol{x}_i + r\boldsymbol{u}$ with $r \in \mathbb{R}_+$ and $\boldsymbol{u} \in \mathcal{S}^2$ in (18) and (19) leads to (21) and (22). □

Appendix B
Proof of Proposition 2

B.1. First order moments

Firstly, equation (23) shows that

$$\mathbb{E}[dN(r)] = 4\pi\lambda r^2 dr. \tag{41}$$

Then equations (22) and (41) imply (24). Moreover, (41) and the change of variable $r = c(t - T - u)$ in (21) prove that:

$$\mathbb{E}[b_i(t)] = 4\pi\lambda c^2 \left(\int_{u=-T}^{t-T} (t - T - u) g(u) du \right). \tag{42}$$

Finally, substituting (15) into (42) shows that $\forall t \geq 2T$, $\mathbb{E}[b_i(t)] = 0$. Then equation (17) implies (25).

B.2. Second order moments

1) In the spectral domain: Firstly, equation (23) shows that

$$\operatorname{cov}[dN(r_1), dN(r_2)] = 4\pi\lambda\, \delta(r_2 - r_1) r_1 r_2 dr_1 dr_2. \tag{43}$$

Then (22) and (43) prove that

$$\begin{aligned} \operatorname{cov}[\mathcal{F}_{h_i}(f_1), \mathcal{F}_{h_i}(f_2)] = \quad & 2\pi\lambda c\, \mathcal{L}_g(\alpha + 2\imath\pi f_1) \\ & \mathcal{L}_g(\alpha + 2\imath\pi f_2) \tfrac{e^{-2\imath\pi(f_1-f_2)T}}{\alpha+\imath\pi(f_1-f_2)}. \end{aligned} \tag{44}$$

Equation (44) implies both (26) and (27).

2) In the time domain: Equations (21) and (43) lead to (28), which jointly proves both (29) and (30). Besides, (28) and (17) imply both (31) and (32).

3) In the time-frequency domain: Finally, substituting (17), (21) and (43) into (11) with $\psi_1 = \psi_2 = h_i$ proves that

$$\mathcal{W}_{h_i,h_i}(t,f) = 4\pi\lambda e^{-2\alpha(t-T)} \int_{r\in\mathbb{R}_+} I(t - T - \frac{r}{c}, f) dr \tag{45}$$

where

$$I(t,f) = \int_{u\in\mathbb{R}} g\left(t + \frac{u}{2}\right) g\left(t - \frac{u}{2}\right) e^{-2\imath\pi f u} du = \mathcal{W}_{g,g}(t,f). \tag{46}$$

In order to conclude, we will use two properties of the Wigner distribution. Firstly, the time support of $\mathcal{W}_{g,g}$ is the same as that of g. Secondly, the *projection property* shows that $\int_{t\in\mathbb{R}} \mathcal{W}_{g,g}(t,f)dt = |\mathcal{F}_g(f)|^2$. Therefore substituting (46) and (30) into (45) finally implies (33).

B.3. Asymptotic normality

Equations (21), (23) and (8) prove that the logarithm of the characteristic function of $b_i(t)$ is $\forall\theta \in \mathbb{R}$,

$$\begin{aligned} \ln(\phi_{b_i(t)}(\theta)) &= \ln(\mathbb{E}[e^{\imath\theta b_i(t)}]) \\ &= 4\pi\lambda \int_{r\in\mathbb{R}_+} \left(e^{\imath\theta \frac{g\left(t-T-\frac{r}{c}\right)}{r}} - 1 \right) r^2 dr \\ &= \sum_{n=1}^{+\infty} \tfrac{(\imath\theta)^n}{n!} \kappa_n(t) \end{aligned} \tag{47}$$

where $\kappa_n(t)$ is the n-th order cumulant of $b_i(t)$:

$$\kappa_n(t) = 4\pi\lambda \int_{r\in\mathbb{R}_+} g\left(t - T - \frac{r}{c}\right)^n r^{2-n} dr. \tag{48}$$

The change of variables $r = c(t - T - u)$ in (48) implies

$$\forall t \geq 2T,\ \kappa_n(t) = 4\pi\lambda c^{3-n} \int_{u=-T}^{T} g(u)^n (t - T - u)^{2-n} du.$$

Therefore, $\forall n \geq 2$, $\forall t > 2T$,

$$|\kappa_n(t)| \leq \frac{4\pi\lambda c^{3-n} \int_{u=-T}^{T} |g(u)|^n du}{(t-2T)^{n-2}}. \tag{49}$$

Let $\varepsilon > 0$. Substituting (49) into (47), we get: $\forall t \geq (2+\varepsilon)T$,

$$\left| \ln(\phi_{b_i(t)}(\theta)) - \left(\imath\theta\kappa_1(t) - \frac{\theta^2}{2}\kappa_2(t) \right) \right| \leq \frac{\psi(\theta)}{t-2T} \underset{t\to+\infty}{\longrightarrow} 0,$$

where $\psi(\theta) = 4\pi\lambda(\varepsilon cT)^3 \int_{u=-T}^{T} \left(e^{\left|\frac{\theta g(u)}{\varepsilon cT}\right|} - \sum_{n=0}^{2} \frac{\left|\frac{\theta g(u)}{\varepsilon cT}\right|^n}{n!} \right) du$.

Therefore the characteristic function of $b_i(t)$ converges pointwise to that of the normal distribution when $t \to +\infty$, which proves that $b_i(t)$ is asymptotically normally distributed. In the same way, it can be proved[10] that the random variables $b_i(t_1) \dots b_i(t_K)$ for all $K \in \mathbb{N}$ and $t_1 \dots t_K \in \mathbb{R}$ are jointly normally distributed when $t \to +\infty$, which shows that $b_i(t)$ is asymptotically distributed as a stationary Gaussian process.

Appendix C
Proof of Proposition 3

C.1. Geometry with two microphones

Let $\boldsymbol{x}_i, \boldsymbol{x}_j \in \mathbb{R}^3$. Let $\xi_1, \xi_2 : \mathbb{R}_+ \to \mathbb{C}$. In the next sections, we will have to compute several integrals of the form:

$$I_{\xi_1,\xi_2} = \int_{\boldsymbol{x}\in\mathbb{R}^3} \frac{\xi_1(\|\boldsymbol{x}-\boldsymbol{x}_i\|_2)}{\|\boldsymbol{x}-\boldsymbol{x}_i\|_2} \frac{\overline{\xi_2(\|\boldsymbol{x}-\boldsymbol{x}_j\|_2)}}{\|\boldsymbol{x}-\boldsymbol{x}_j\|_2} d\boldsymbol{x}. \tag{50}$$

To compute such an integral, we will use the spherical coordinates (r,θ,φ), as illustrated in Fig. 4, where $\theta = 0$ corresponds to the direction of vector $\boldsymbol{x}_j - \boldsymbol{x}_i$. We thus get $\boldsymbol{x} = [r\cos(\theta)\cos\varphi, r\cos(\theta)\sin\varphi, r\sin(\theta)]^\top$ and $d\boldsymbol{x} =$

[10] The proof is the same and it is omitted here for the sake of conciseness.

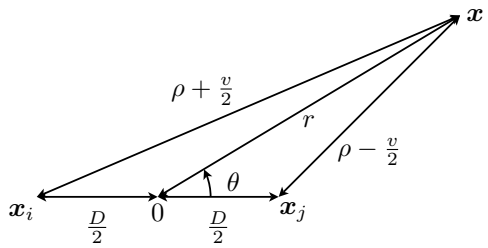

Fig. 4. Geometry with two microphones at $\boldsymbol{x}_i$, $\boldsymbol{x}_j$ and a source image at $\boldsymbol{x}$

$r^2 dr \sin(\theta) d\theta d\varphi$, with $r \in \mathbb{R}_+$, $\theta \in [0, \pi]$ and $\varphi \in [0, 2\pi]$. Moreover, as can be seen in Fig. 4, we have

- $\|\boldsymbol{x} - \boldsymbol{x}_i\|_2 = \sqrt{r^2 + \frac{D^2}{4} + rD\cos(\theta)}$,
- $\|\boldsymbol{x} - \boldsymbol{x}_j\|_2 = \sqrt{r^2 + \frac{D^2}{4} - rD\cos(\theta)}$.

By substitution into (50), we get

$$I_{\xi_1,\xi_2} = 2\pi \int_{r=0}^{+\infty} \int_{\theta=0}^{\pi} \frac{\xi_1\left(\sqrt{r^2+\frac{D^2}{4}+rD\cos(\theta)}\right)}{\sqrt{r^2+\frac{D^2}{4}+rD\cos(\theta)}} \frac{\xi_2\left(\sqrt{r^2+\frac{D^2}{4}-rD\cos(\theta)}\right)}{\sqrt{r^2+\frac{D^2}{4}-rD\cos(\theta)}} r^2 dr \sin(\theta) d\theta. \tag{51}$$

Finally, we make a last change of variables, that is also illustrated in Fig. 4:

$$\begin{aligned} \rho &= \frac{\|\boldsymbol{x}-\boldsymbol{x}_i\|_2 + \|\boldsymbol{x}-\boldsymbol{x}_j\|_2}{2} \\ &= \frac{\sqrt{r^2+\frac{D^2}{4}+rD\cos(\theta)} + \sqrt{r^2+\frac{D^2}{4}-rD\cos(\theta)}}{2}, \\ v &= \|\boldsymbol{x}-\boldsymbol{x}_i\|_2 - \|\boldsymbol{x}-\boldsymbol{x}_j\|_2 \\ &= \sqrt{r^2+\frac{D^2}{4}+rD\cos(\theta)} - \sqrt{r^2+\frac{D^2}{4}-rD\cos(\theta)}, \end{aligned}$$

which is such that $\rho \in \left[\frac{D}{2}, +\infty\right[$, $v \in [-D, D]$, and

$$\frac{r^2 dr \sin(\theta) d\theta}{\sqrt{r^2+\frac{D^2}{4}+rD\cos(\theta)}\sqrt{r^2+\frac{D^2}{4}-rD\cos(\theta)}} = \frac{d\rho dv}{D}.$$

Equation (51) thus becomes

$$I_{\xi_1,\xi_2} = \frac{2\pi}{D} \int_{\rho=\frac{D}{2}}^{+\infty} \int_{v=-D}^{D} \xi_1\left(\rho + \frac{v}{2}\right) \overline{\xi_2\left(\rho - \frac{v}{2}\right)} d\rho dv. \tag{52}$$

C.2. In the spectral domain

Firstly, equation (14) shows that

$$\operatorname{cov}[dN(\boldsymbol{x}_1), dN(\boldsymbol{x}_2)] = \lambda\, \delta(\boldsymbol{x}_2 - \boldsymbol{x}_1) d\boldsymbol{x}_1 d\boldsymbol{x}_2. \tag{53}$$

Then (19) and (53) show that

$$\operatorname{cov}[\mathcal{F}_{h_i}(f_1), \mathcal{F}_{h_j}(f_2)] = \lambda \mathcal{L}_g(\alpha + 2\imath\pi f_1)\mathcal{L}_g(\alpha + 2\imath\pi f_2) e^{-2\imath\pi(f_1-f_2)T} I_{\xi_1,\xi_2}, \tag{54}$$

where $\xi_1(r) = e^{-\frac{\alpha+2\imath\pi f_1}{c}r}$, $\xi_2(r) = e^{-\frac{\alpha+2\imath\pi f_2}{c}r}$, and I_{ξ_1,ξ_2} was defined in (50). Then equation (52) shows that

$$\begin{aligned} I_{\xi_1,\xi_2} &= \frac{2\pi}{D} \int_{\rho=\frac{D}{2}}^{+\infty} e^{-2\frac{\alpha+\imath\pi(f_1-f_2)}{c}\rho} d\rho \int_{v=-D}^{D} e^{-2\imath\pi\frac{f_1+f_2}{2c}v} dv \\ &= 2\pi c \frac{e^{-\frac{\alpha+\imath\pi(f_1-f_2)}{c}D}}{\alpha+\imath\pi(f_1-f_2)} \operatorname{sinc}\left(2\pi\tfrac{f_1+f_2}{2c}D\right). \end{aligned} \tag{55}$$

By substituting (55) and (26) into (54), we finally get (35).

C.3. In the time domain

Equations (18) and (53) imply

$$\operatorname{cov}[b_i(t_1), b_j(t_2)] = \lambda I_{\xi_1,\xi_2} \tag{56}$$

where $\xi_1(r) = g\left(t_1 - T - \frac{r}{c}\right)$, $\xi_2(r) = g\left(t_2 - T - \frac{r}{c}\right)$, and I_{ξ_1,ξ_2} was defined in (50). Then substituting (52) into (56) shows that

$$\operatorname{cov}[b_i(t_1), b_j(t_2)] = 4\pi\lambda \int_{\rho=\frac{D}{2}}^{+\infty} I(t_1 - T - \tfrac{\rho}{c}, t_2 - T - \tfrac{\rho}{c}) d\rho \tag{57}$$

where

$$I(t_1, t_2) = \frac{1}{2D} \int_{v=-D}^{D} g\left(t_1 - \tfrac{v}{2c}\right) g\left(t_2 + \tfrac{v}{2c}\right) dv. \tag{58}$$

With $v = cu$, substituting (34) into (58) proves that

$$I(t_1, t_2) = \int_{u\in\mathbb{R}} g\left(t_1 - \frac{u}{2}\right) g\left(t_2 + \frac{u}{2}\right) w(u) du. \tag{59}$$

Substituting (59) into (57) proves (36), which with (29) implies (37). Moreover, applying the Fourier transform (9) to (36) and substituting (30) leads to (38).

Then (17) and (36) prove that

$$\operatorname{cov}[h_i(t_1), h_j(t_2)] = 4\pi\lambda c e^{-2\alpha(\frac{t_1+t_2}{2}-T)} w * \widetilde{g} * g\,(t_1 - t_2)\,. \tag{60}$$

Finally, substituting (31) and (29) into (60) implies (39).

C.4. In the time-frequency domain

Substituting (17), (18) and (53) into (11) with $\psi_1 = h_i$ and $\psi_2 = h_j$ implies

$$\mathcal{W}_{h_i,h_j}(t, f) = \lambda e^{-2\alpha(t-T)} \int_{\mathbb{R}} I_{\xi_1,\xi_2} e^{-2\imath\pi f u} du. \tag{61}$$

where $\xi_1(r) = g\left(t + \frac{u}{2} - T - \frac{r}{c}\right)$, $\xi_2(r) = g\left(t - \frac{u}{2} - T - \frac{r}{c}\right)$, and I_{ξ_1,ξ_2} was defined in (50).

Then substituting (52) into (61) shows that

$$\mathcal{W}_{h_i,h_j}(t, f) = \frac{4\pi\lambda e^{-2\alpha(t-T)}}{2D} \int_{\rho=\frac{D}{2}}^{+\infty} \int_{v=-D}^{D} I(t - T - \tfrac{\rho}{c}, f, v) d\rho dv \tag{62}$$

with

$$\begin{aligned} I(t, f, v) &= \int_{u\in\mathbb{R}} g\left(t + \tfrac{u}{2} - \tfrac{v}{2c}\right) g\left(t - \tfrac{u}{2} + \tfrac{v}{2c}\right) e^{-2\imath\pi f u} du \\ &= e^{-2\imath\pi f \frac{v}{c}} \mathcal{W}_{g,g}\,(t, f)\,, \end{aligned} \tag{63}$$

where $\mathcal{W}_{g,g}(t,f)$ was expressed in (46), and we have used the change of variable $u' = u - \frac{v}{c}$.

In order to conclude, we will use the two properties of the Wigner distribution that we already used in Section B.2.3). Firstly, the time support of $\mathcal{W}_{g,g}$ is the same as that of g. Secondly, $\int_{t\in\mathbb{R}} \mathcal{W}_{g,g}(t,f)dt = |\mathcal{F}_g(f)|^2$. Substituting (63) and (30) into (62) finally implies (40).

C.5. Asymptotic normality

Let $\boldsymbol{b}(t) = [b_i(t), b_j(t)]^\top$ and $\boldsymbol{\theta} = [\theta_1, \theta_2]^\top$. Equations (18), (14) and (8) prove that the logarithm of the characteristic function of $\boldsymbol{b}(t)$ is

$$\begin{aligned} & \ln(\phi_{\boldsymbol{b}(t)}(\theta)) \\ = \; & \ln(\mathbb{E}[e^{\imath(\theta_1 b_i(t) + \theta_2 b_j(t))}]) \\ = \; & \lambda \int_{\boldsymbol{x}\in\mathbb{R}^3} (e^{\imath(\theta_1 \frac{g(t-T-\frac{\|\boldsymbol{x}-\boldsymbol{x}_i\|_2}{c})}{\|\boldsymbol{x}-\boldsymbol{x}_i\|_2} + \theta_2 \frac{g(t-T-\frac{\|\boldsymbol{x}-\boldsymbol{x}_j\|_2}{c})}{\|\boldsymbol{x}-\boldsymbol{x}_j\|_2})} - 1) d\boldsymbol{x} \\ = \; & \sum_{n=1}^{+\infty} \frac{\imath^n}{n!} \sum_{k=0}^{n} \binom{n}{k} \theta_1^k \theta_2^{n-k} \kappa_{k,n-k}(t) \end{aligned} \tag{64}$$

where $\kappa_{n_1,n_2}(t)$ is the (n_1,n_2)-th order cumulant of $\boldsymbol{b}(t)$:

$$\kappa_{n_1,n_2}(t) = \lambda I_{\xi_1,\xi_2}, \tag{65}$$

where $\xi_1(r) = \frac{\left(g\left(t-T-\frac{r}{c}\right)\right)^{n_1}}{r^{n_1-1}}$, $\xi_2(r) = \frac{\left(g\left(t-T-\frac{r}{c}\right)\right)^{n_2}}{r^{n_2-1}}$, and I_{ξ_1,ξ_2} was defined in (50).

Then substituting (52) into (65) shows that

$$\begin{aligned} \kappa_{n_1,n_2}(t) = \; & \frac{2\pi\lambda}{D} \int_{\rho=\frac{D}{2}}^{+\infty} \int_{v=-D}^{D} \frac{\left(g\left(t-T-\frac{\rho+\frac{v}{2}}{c}\right)\right)^{n_1}}{(\rho+\frac{v}{2})^{n_1-1}} \\ & \frac{\left(g\left(t-T-\frac{\rho-\frac{v}{2}}{c}\right)\right)^{n_2}}{(\rho-\frac{v}{2})^{n_2-1}} d\rho dv. \end{aligned} \tag{66}$$

The change of variables $\rho = c(t-T-u)$ and $v = cw$ in (66) implies that $\forall t \geq 2T + \frac{D}{c}$,

$$\begin{aligned} \kappa_{n_1,n_2}(t) = \; & \frac{2\pi\lambda c^{4-n_1-n_2}}{D} \int_{u\in\mathbb{R}} \int_{w=-\frac{D}{c}}^{\frac{D}{c}} \frac{\left(g\left(u-\frac{w}{2}\right)\right)^{n_1}}{(t-T-u+\frac{w}{2})^{n_1-1}} \\ & \frac{\left(g\left(u+\frac{w}{2}\right)\right)^{n_2}}{(t-T-u-\frac{w}{2})^{n_2-1}} du dw. \end{aligned}$$

Therefore $\forall n_1+n_2 \geq 2$, $\forall t \geq 2T + \frac{D}{c}$,

$$\begin{aligned} |\kappa_{n_1,n_2}(t)| \leq \; & \frac{2\pi\lambda c^{4-n_1-n_2}}{D} \\ & \frac{\int_{u\in\mathbb{R}} \int_{w=-\frac{D}{c}}^{\frac{D}{c}} \left|g\left(u-\frac{w}{2}\right)\right|^{n_1} \left|g\left(u+\frac{w}{2}\right)\right|^{n_2} du dw}{(t-2T)^{n_1+n_2-2}}. \end{aligned} \tag{67}$$

Substituting (67) into (64), we get $\forall t \geq 2T + \frac{D}{c}$,

$$\begin{aligned} & \left| \ln(\phi_{\boldsymbol{b}(t)}(\theta)) - \sum_{n=1}^{2} \frac{\imath^n}{n!} \sum_{k=0}^{n} \binom{n}{k} \theta_1^k \theta_2^{n-k} \kappa_{k,n-k}(t) \right| \\ \leq \; & \frac{1}{(t-2T)} \psi(\theta_1,\theta_2) \underset{t\to+\infty}{\longrightarrow} 0, \end{aligned}$$

where

$$\begin{aligned} \psi(\theta_1,\theta_2) = \; & 2\pi\lambda c D^2 \int_{u\in\mathbb{R}} \int_{w=-\frac{D}{c}}^{\frac{D}{c}} e^{\frac{\left|\theta_1 g\left(u-\frac{w}{2}\right)\right| + \left|\theta_2 g\left(u+\frac{w}{2}\right)\right|}{D}} \\ & - \sum_{n=0}^{2} \frac{1}{n!} \left(\frac{\left|\theta_1 g\left(u-\frac{w}{2}\right)\right| + \left|\theta_2 g\left(u+\frac{w}{2}\right)\right|}{D} \right)^n du dw. \end{aligned}$$

Therefore the characteristic function of $\boldsymbol{b}(t)$ converges pointwise to that of the normal distribution when $t \to +\infty$, which proves that $\boldsymbol{b}(t)$ is asymptotically normally distributed. In the same way, it can be proved[11] that the random variables $\boldsymbol{b}(t_1)\dots\boldsymbol{b}(t_K)$ for all $K \in \mathbb{N}$ and $t_1 \dots t_K \in \mathbb{R}$ are jointly normally distributed when $t \to +\infty$, which proves that $\boldsymbol{b}(t)$ is asymptotically distributed as a stationary Gaussian process.

ACKNOWLEDGMENTS

Ahead of this work, I had some very interesting and inspiring discussions about reverberation with several persons that I would like to thank here, including my former PhD students Simon Leglaive and Arthur Belhomme, and my colleagues Gaël Richard, Yves Grenier, Laurent Girin, Antoine Liutkus, Philippe Depalle and Xavier Boutillon.

REFERENCES

[1] H. Kuttruff, *Room Acoustics, Fifth Edition*. CRC Press, 2014.
[2] J.-D. Polack, "Modifying chambers to play billiards: the foundations of reverberation theory," *Acta Acustica united with Acustica*, vol. 76, no. 6, pp. 256–272(17), Jul. 1992.
[3] ——, "Playing billiards in the concert hall: The mathematical foundations of geometrical room acoustics," *Applied Acoustics*, vol. 38, no. 2, pp. 235 – 244, 1993.
[4] R. Balian and C. Bloch, "Distribution of eigenfrequencies for the wave equation in a finite domain: I. three-dimensional problem with smooth boundary surface," *Annals of Physics*, vol. 60, no. 2, pp. 401–447, 1970.
[5] M. R. Schroeder, "Frequency-correlation functions of frequency responses in rooms," *The Journal of the Acoustical Society of America*, vol. 34, no. 12, pp. 1819–1823, 1962.
[6] M. R. Schroeder and K. H. Kuttruff, "On frequency response curves in rooms. comparison of experimental, theoretical, and Monte Carlo results for the average frequency spacing between maxima," *The Journal of the Acoustical Society of America*, vol. 34, no. 1, pp. 76–80, 1962.
[7] M. R. Schroeder, "Statistical parameters of the frequency response curves of large rooms," *The Journal of the Acoustical Society of America*, vol. 35, no. 5, pp. 299–306, 1987.
[8] J.-M. Jot, L. Cerveau, and O. Warusfel, "Analysis and synthesis of room reverberation based on a statistical time-frequency model," in *Audio Engineering Society Convention 103*, Sep 1997.
[9] A. Baskind, "Modèles et méthodes de description spatiale de scènes sonores : application aux enregistrements binauraux," Ph.D. dissertation, Université Pierre et Marie Curie (UPMC), Paris, France, 2003.
[10] T. Schultz, "Diffusion in reverberation rooms," *Journal of Sound and Vibration*, vol. 16, no. 1, pp. 17 – 28, 1971.
[11] W. B. Joyce, "Sabine's reverberation time and ergodic auditoriums," *The Journal of the Acoustical Society of America*, vol. 58, no. 3, pp. 643–655, 1975.
[12] L. Cremer, H. A. Muller, and T. J. Schultz, *Principles and Applications of Room Acoustics - Volume 1*. Applied Science Publishers Ltd, 1982.
[13] J. A. Moorer, "About this reverberation business," *Computer Music Journal*, vol. 3, no. 2, pp. 13–28, 1979.
[14] R. K. Cook, R. V. Waterhouse, R. D. Berendt, S. Edelman, and M. C. Thompson Jr., "Measurement of correlation coefficients in reverberant sound fields," *The Journal of the Acoustical Society of America*, vol. 27, no. 6, pp. 1072–1077, 1955.
[15] F. Jacobsen and T. Roisin, "The coherence of reverberant sound fields," *The Journal of the Acoustical Society of America*, vol. 108, no. 1, pp. 204–210, 2000.
[16] G. W. Elko, "Spatial coherence functions for differential microphones in isotropic noise fields," *Mcrophone arrays*, pp. 61–85, 2001.
[17] J. D. Polack, "La transmission de l'énergie sonore dans les salles," Ph.D. dissertation, Université du Maine, 1988.
[18] L. Cohen, "Time-frequency distributions-a review," *Proc. IEEE*, vol. 77, no. 7, pp. 941–981, Jul 1989.
[19] S. N. Chiu, D. Stoyan, W. S. Kendall, and J. Mecke, *Stochastic Geometry and Its Applications*, 3rd ed. Wiley, 2013.
[20] J. B. Allen and D. A. Berkley, "Image method for efficiently simulating small-room acoustics," *Journal of the Acoustical Society of America*, vol. 65, no. 4, pp. 943–950, 1 1979.

[11] The proof is the same and it is omitted here for the sake of conciseness.

Dépôt légal : 2018 – 1er trimestre
Imprimé à Télécom ParisTech – Paris
ISSN 0751-1345 ENST D (Paris) (France 1983-9999)

Télécom ParisTech

Institut Mines-Télécom - membre de l'Université Paris Saclay

46, rue Barrault - 75634 Paris Cedex 13 - Tél. + 33 (0)1 45 81 77 77 - www.telecom-paristech.fr

Département IDS